

# Adapting the Lanczos algorithm to matrices with almost continuous spectra

Jörn Zimmerling<sup>1\*</sup> and Vladimir Druskin<sup>2,3†</sup>

<sup>1</sup>Institutionen för informationsteknologi, Uppsala Universitet,  
Lägerhyddsvägen 2, Uppsala, 752 37, Uppsala, Sweden.

<sup>2</sup>Department of Mathematical Sciences, Worcester Polytechnic  
Institute, 100 Institute Road, Worcester, 01609, MA, USA.

<sup>3</sup>Department of Mathematics, Southern Methodist University, 3100  
Dyer St, Clements Hall Room 208, Dallas, 75205, TX, USA.

\*Corresponding author(s). E-mail(s): [jorn.zimmerling@it.uu.se](mailto:jorn.zimmerling@it.uu.se);

Contributing authors: [vdruskin@gmail.com](mailto:vdruskin@gmail.com);

†These authors contributed equally to this work.

## Abstract

We consider the approximation of  $\mathbf{B}^T(\mathbf{A} + s\mathbf{I})^{-1}\mathbf{B}$  where  $\mathbf{A} \in \mathbb{R}^{n \times n}$  is large, symmetric positive definite, and has a dense spectrum, and  $\mathbf{B} \in \mathbb{R}^{n \times p}$ ,  $p \ll n$ . Our target application is the computation of Multiple-Input Multiple-Output transfer functions arising from large-scale discretizations of problems with continuous spectral measures, such as linear time-invariant PDEs on unbounded domains. Traditional Krylov methods, such as Lanczos or conjugate gradients, focus on resolving individual eigenvalues of a dense discretization, while ignoring the underlying continuous spectral measure that these points approximate. We argue that it is more efficient to model the inherent branch cut of the original operator than to exhaustively resolve the artificial point spectrum induced by discretization. We place this problem in a more general framework, known in the physics literature of the 1970s as the square-root terminator or recursion method. This framework accelerates Lanczos recursions for the computation of Green's functions and spectral densities in problems with continuous spectral measures, leading to dramatic speedups when the recursion reaches a stationary limit. However, this stationarity condition is generally not satisfied for matrices arising from the discretization of PDEs on unbounded domains. To overcome this obstacle, we formulate the quadratic terminator in the framework of Krein–Nudelman semi-infinite strings, with parameters chosen adaptively by maximizing relative energy

outflow. This approach results in a low-rank modification to the (block) Lanczos matrix, dependent on  $\sqrt{s}$ , with an additional  $O(n)$  cost. We demonstrate significant error reductions for large-scale self-adjoint PDE discretizations in unbounded domains, including two- and three-dimensional Maxwell's equations in diffusive regimes. The method proves particularly advantageous in computing state-space solutions for wave propagation, specifically for 2D wave and 3D Maxwell's operators. Implicitly replacing the conventional Lanczos spectral decomposition with a representation in terms of the continuous Krein-Nudelman spectrum, we obtain a qualitative improvement in finite-difference approximations, effectively transforming standing-wave artifacts into outgoing propagating waves.

**Keywords:** Block Lanczos, acceleration, quadrature, scattering poles, Krein-Nudelman, square-root terminator, unbounded domains, absorbing boundary conditions

**MSC Classification:** 65F10, 65N22, 65F50, 65F60

# 1 Introduction

## 1.1 Problem statement

Let  $A = A^T \in \mathbb{R}^{n \times n}$  be a symmetric positive definite (s.p.d.) matrix and let  $B$  be a tall matrix with  $B \in \mathbb{R}^{n \times p}$ , with  $p \ll n$ . We refer to  $p$  as the size of the block. We target the approximation of the square multi-input multi-output (MIMO) transfer function

$$\mathcal{F}(s) = B^T(A + sI)^{-1}B, \quad (1)$$

for  $s \in \mathbb{C} \setminus (-\infty, 0)$  outside the spectrum  $A$ . Generally,  $\mathcal{F}(s) \in \mathbb{C}^{p \times p}$  is a complex symmetric matrix-valued function and it becomes s.p.d. for real positive  $s$ . We compute the matrix quadratic form (1) via the block Krylov subspace

$$\mathcal{K}_m(A, B) := \text{blkspan}\{B, AB, A^2B, \dots, A^{m-1}B\},$$

where blkspan means that the whole space range ( $[B, AB, A^2B, \dots, A^{m-1}B]$ ) is generated. To simplify notation, without loss of generality, we assume that the matrix  $B$  has orthonormal columns. Conventionally, the (block) Krylov subspace approximations of matrix quadratic forms (1) are computed via (block)-Gaußian quadratures, e.g., [1–3]. The efficiency of such an approach follows from the shifted energy norm optimality of the Lanczos approximations for  $s \in \mathbb{R}_+$  and near-optimality for  $f(A)B$  for general  $f$  [4] yielding adaptation to coarse nonuniform spectral distributions; however, this property weakens on intervals of dense uniform spectra. An error improvement of about one order of magnitude for a given  $m$  was obtained in [5] by averaging block Gauß and block Gauß-Radau quadratures. Combinations of such quadratures were used for tight two-sided bounds [5–8], such that averaging naturally leads to a more accurate estimate.

Here we adapt a more general approach used in quantum physics for acceleration of the Lanczos algorithm for Green function calculation and spectral density estimations for problems with continuum spectra, e.g., see [9–14]. It is based on the assumption that the Lanczos recursion converges to a stationary limit, thus asymptotically it becomes a shifted Chebyshev recursion. A spectral function of such a recursion can be expressed via a Stieltjes continued-fraction (S-fraction) whose coefficients converge. Such a S-fraction can be exactly truncated via a function in the form  $b\sqrt{s(s-a)}$ . That is the infinite S-fraction with coefficient  $\gamma$  and  $s\hat{\gamma}$  gives

$$\frac{\gamma}{2} + \frac{1}{s\hat{\gamma} + \frac{1}{\gamma + \frac{1}{s\hat{\gamma} + \dots}}} = \frac{\gamma}{2s} \sqrt{s \left( s + \frac{4}{\gamma\hat{\gamma}} \right)}, \quad (2)$$

hence the name square-root terminator or recursion method. The intuition behind such a modification is the description of continuous spectra via scattering poles or resonances (residing on the second Riemann sheet) in unbounded domains [15]. In quantum-mechanical computations the coefficient of a Schrödinger potential is often given analytically, in which case the Lanczos recursion is performed in closed form with exponentially growing complexity; that is why the square root termination allowed physicists to solve otherwise non-tractable problems.

However, this powerful approach has seen limited use in the computational linear algebra community, as its core assumption on the recursion limit is overly restrictive and may break down in the presence of intervals of nonuniform spectral distributions. This issue is exacerbated by numerical instability in the commonly used simple Lanczos algorithm without reorthogonalization.

Here, we overcome that limitation by using extensions of the Stieltjes string theory developed by Mark Krein and his school. The derivation of block Gauß–Radau formulas in [5] was based on the connection of the block Lanczos algorithm to the block extension of discrete Stieltjes strings and block Stieltjes continued fraction. The scalar variant of this connection was introduced in the seminal work by Mark Krein in the 1950s, e.g., see [16–18]. An extension of this approach for problems with continuous spectra was introduced by Krein and Nudelman [19] by adding a damper at the end of the Stieltjes string. Here we use this approach by adaptively modifying the block Lanczos recursion to move poorly convergent Ritz values to the other Riemann sheet, while still matching the same number of spectral moments as in the conventional block Lanczos method. The free parameter (damper) of such an extension is chosen from maximization of the damped energy (energy outflow) relative to the energy stored in the system, thus maximizing spectral deformation to the other Riemann sheet and smoothness of the spectral measure. This not only accelerates convergence of the transfer function but also removes artifacts of the non-absorbing finite-difference approximation in the exterior (for the state representation for the wave propagation problems in unbounded domains), by transforming standing waves to the outgoing ones, propagating according to d’Alembert characteristics.

The remainder of the article is organized as follows: we review the basic properties of the block Gauß quadrature computed via the block Lanczos algorithm, its connection to Stieltjes strings and representation via truncated Stieltjes-matrix continued

fraction in section 2; In section 3 we extend block Stieltjes strings/continued fractions to, respectively, Krein–Nudelman strings/continued fractions. We further map back the Krein–Nudelman extension in terms of the Lanczos block tridiagonal matrix. Then we discuss the adaptive choice of the Krein–Nudelman parameters, optimizing the regularity of the spectral density, showing that Gauß and Gauß–Radau quadratures are two limiting cases of the Krein–Nudelman extension, and derive a two-sided error bound for the latter for  $s \in \mathbb{R}^+$ . In section 4 we develop an adaptive spectral optimization algorithm to determine Krein–Nudelman parameters based on maximization of the dissipated energy relative to the storage energy of the dynamic system along the negative real axis. The numerical examples are presented in section 5. In conclusion, we outline our outlook for further research.

## 1.2 Notation

Given two square s.p.d. matrices  $G_1, G_2$  we use the notation  $G_1 < G_2$  to mean that the matrix  $G_2 - G_1$  is positive definite (i.e., Löwner ordering). A sequence of matrices  $\{G_m\}_{m \geq 0}$  is said to be monotonically increasing (resp. decreasing) if  $G_m < G_{m+1}$  (resp.  $G_{m+1} < G_m$ ) for all  $m$ . Definite  $p \times p$  matrices are denoted by Greek letters  $\alpha, \beta, \gamma$  and matrix-valued functions by calligraphic capital letters such as  $\mathcal{C}(s)$  or  $\mathcal{F}(s)$ . For  $\alpha, \beta \in \mathbb{R}^{p \times p}$  and  $\beta$  is nonsingular, we use the notation  $\frac{\alpha}{\beta} := \alpha\beta^{-1}$  to denote right inversion. We write  $\frac{1}{A}$  in place of  $\frac{I_p}{A}$  whenever no ambiguity arises, in order to improve readability, especially in continued fractions. The matrix  $E_k \in \mathbb{R}^{mp \times p}$  has zero elements except for the  $p \times p$  identity matrix in the  $k$ -th block,  $E_k = [0, \dots, 0, I, \dots, 0]^T$ . Finally, the imaginary unit is denoted as  $\iota$  to distinguish it from indices  $i, j, k$ .

## 2 Block Gaußian Quadratures, Stieltjes strings and continued fractions

---

### Algorithm 1 Block Lanczos iteration

---

Given  $m, A \in \mathbb{R}^{n \times n}$  s.p.d.,  $B \in \mathbb{R}^{n \times p}$  with orthonormal columns

$$\begin{aligned}
 Q_1 &= B & \triangleright \beta_1 = I_p \text{ as } B^T B = I \\
 W &= A Q_1 \\
 \alpha_1 &= Q_1^T W \\
 W &= W - Q_1 \alpha_1 \\
 \text{for } i &= 2, \dots, m \text{ do} \\
 Q_i \beta_i &= W & \triangleright \text{QR decomposition of } W \\
 W &= A Q_i - Q_{i-1} \beta_i^T \\
 \alpha_i &= Q_i^T W \\
 W &= W - Q_i \alpha_i \\
 \text{end for}
 \end{aligned}$$


---

Let us assume that we can perform  $m$  steps, with  $mp \leq n$ , of the block Lanczos iteration (Algorithm 1) without breakdowns or deflation [20, 21]. As a result, the orthonormal block vectors  $Q_i \in \mathbb{R}^{n \times p}$  form the matrix  $\mathbf{Q}_m = [Q_1, \dots, Q_m] \in \mathbb{R}^{n \times mp}$ , whose columns contain an orthonormal basis for the block Krylov subspace

$$\mathcal{K}_m(A, B) := \text{blkspan}\{B, AB, A^2B, \dots, A^{m-1}B\}.$$

In addition, let us assume that after  $m$  steps one can compute the QR decomposition  $Q_{m+1}\beta_{m+1} = W$  with full rank, where  $W$  is computed on the  $m$ -th step. The Lanczos recursion (with  $m$  multiplications by  $A$ ) can then be compactly written as

$$A\mathbf{Q}_m = \mathbf{Q}_m T_m + Q_{m+1}\beta_{m+1} E_m^T, \quad (3)$$

where  $T_m$  is the s.p.d. block tridiagonal matrix

$$T_m = \begin{pmatrix} \alpha_1 & \beta_2^T \\ \beta_2 & \alpha_2 & \beta_3^T \\ & \ddots & \ddots & \ddots \\ & & \beta_i & \alpha_i & \beta_{i+1}^T \\ & & & \ddots & \ddots \\ & & & & \beta_{m-1} & \alpha_{m-1} & \beta_m^T \\ & & & & & \beta_m & \alpha_m \end{pmatrix}, \quad (4)$$

and  $\alpha_i, \beta_i \in \mathbb{R}^{p \times p}$  are the block coefficients in Algorithm 1.

Using the Lanczos decomposition,  $\mathcal{F}(s)$  can be approximated as

$$\mathcal{F}(s) \approx \mathcal{F}_m(s) = E_1^T (T_m + sI)^{-1} E_1. \quad (5)$$

This approximation is known as a block Gauß quadrature rule matching the matrix moments  $\{B^T A^i B\}_{i=0}^{2m-1}$  [22].

The simple Lanczos algorithm using only three-term recursions without re-orthogonalization is known to be unstable due to computer round-offs. The instability is manifested by the loss of orthogonality of the Lanczos vectors and the appearance of spurious copies of the Lanczos eigenvalues. However, this instability only slows down the convergence speed to some degree and does not affect the accuracy of the final converged result [23, 24].

To interpret the system as a block extension of Stieltjes strings, we apply a block  $LDL^T$  decomposition to  $T_m$  (as defined in equation (4)), following the approach established in [5]. This results in

$$T_m := (\widehat{\mathbf{K}}_m^{-1})^T J_m \Gamma_m^{-1} J_m^T \widehat{\mathbf{K}}_m^{-1} \quad (6)$$

where  $\widehat{\kappa}_i \in \mathbb{R}^{p \times p}$ ,  $\widehat{\kappa}_1 = I_p$  and  $\gamma_i \in \mathbb{R}^{p \times p}$  are all full rank,

$$J_m^T = \begin{bmatrix} I_p & -I_p & & \\ & \ddots & \ddots & \\ & & \ddots & -I_p \\ & & & I_p \end{bmatrix} \in \mathbb{R}^{pm \times pm}, \quad \widehat{\kappa}_m = \text{blkdiag}(\widehat{\kappa}_1, \dots, \widehat{\kappa}_m), \\ \Gamma_m = \text{blkdiag}(\gamma_1, \dots, \gamma_m),$$

and  $\alpha_1 = (\widehat{\kappa}_1^{-1})^T \gamma_1^{-1} \widehat{\kappa}_1^{-1} = \gamma_1^{-1}$ ,  $\alpha_i = (\widehat{\kappa}_i^{-1})^T (\gamma_{i-1}^{-1} + \gamma_i^{-1}) \widehat{\kappa}_i^{-1}$  and  $\beta_i = -(\widehat{\kappa}_i^{-1})^T \gamma_{i-1}^{-1} \widehat{\kappa}_{i-1}^{-1}$  for  $i = 2, \dots, m$ .

The matrices  $\gamma_i$  and  $\widehat{\kappa}_i$  can be computed directly during the block Lanczos recursion using the coefficients  $\alpha_i$ 's and  $\beta_i > 0$ 's using Algorithm 2, given in Appendix A, and previously derived for a different parametrization in [25].

We first convert  $T_m$  to pencil form using the  $LDL^T$  factors introduced in decomposition (6). To this end, we introduce the matrices  $\widehat{\gamma}_j$

$$\widehat{\gamma}_j = \widehat{\kappa}_j^T \widehat{\kappa}_j, \quad j = 1, \dots, m. \quad (7)$$

The matrices  $\gamma_j$  and  $\widehat{\gamma}_j$  are known as the Stieltjes parameters, and they are both s.p.d. if block Lanczos runs without breakdown. While  $\widehat{\kappa}_j$ 's depend on the choice of block-orthogonalization used in the block Lanczos algorithm, the Stieltjes parameters do not.

Let  $Z_m := J_m \Gamma_m^{-1} J_m^T$  and  $\widehat{\Gamma}_m = \text{blkdiag}(\widehat{\gamma}_1, \dots, \widehat{\gamma}_m)$ . Then, due to  $B^T B = I_p$ , the initial parameter  $\widehat{\gamma}_1 = I_p$  and the approximation  $\mathcal{F}_m$  of the transfer-function  $\mathcal{F} = B^T (A + sI)^{-1} B$  can be expressed using the pencil  $(Z_m, \widehat{\Gamma}_m)$  as

$$\mathcal{F}_m(s) = E_1^T (T_m + sI)^{-1} E_1 = E_1^T (Z_m + s\widehat{\Gamma}_m)^{-1} E_1. \quad (8)$$

Thus  $\mathcal{F}_m(s)$  corresponds to the first  $p \times p$  block of the solution  $U_m \in \mathbb{C}^{mp \times p}$  of the linear system

$$(Z_m + s\widehat{\Gamma}_m) U_m = E_1, \quad (9)$$

with block column vector  $U_m = [\mathcal{U}_1; \dots; \mathcal{U}_m]$ , with  $\mathcal{U}_i$  a  $p \times p$  block.

By augmenting  $U_m$  with the ‘‘boundary’’ blocks  $\mathcal{U}_0, \mathcal{U}_{m+1} \in \mathbb{C}^{p \times p}$  and introducing the fictitious term  $\gamma_0 = I_p$ , we can rewrite (9) as a block (finite-difference) Stieltjes string

$$\frac{1}{\gamma_0} (\mathcal{U}_1 - \mathcal{U}_0) = -I_p \quad (10)$$

$$\frac{1}{\gamma_{i-1}} (\mathcal{U}_i - \mathcal{U}_{i-1}) - \frac{1}{\gamma_i} (\mathcal{U}_{i+1} - \mathcal{U}_i) + s\widehat{\gamma}_i \mathcal{U}_i = \mathbf{0}, \quad i = 1, \dots, m \quad (11)$$

$$\mathcal{U}_{m+1} = \mathbf{0}. \quad (12)$$

where the first line can be interpreted as a block Neumann condition and the last as a block Dirichlet condition.

For  $p = 1$  Krein [17] interpreted the system (10-12) as a so-called Stieltjes string

$$-u_{xx} + s\mathbf{m}_m(x)u = 0 \quad (13)$$

on a positive interval  $[0, x_{m+1}]$ , with boundary conditions  $u_x(0) = -1$ ,  $u(x_{m+1}) = 0$ , and discrete mass distribution

$$\mathbf{m}_m(x) = \sum_{i=1}^m \hat{\gamma}_i \delta(x - x_i), \quad (14)$$

where  $x_1 = 0$ ,  $x_{i+1} = x_i + \gamma_i$ ,  $i = 1, \dots, m$ , with  $\mathcal{U}_i = u(x_i)$  (see [26] for a detailed derivation). The discrete Stieltjes string interpretation is fundamental for the derivation of our algorithm.

The eigendecomposition of  $T_m$  traditionally links  $\mathcal{F}_m(s)$  to block Gaußian quadrature [27]; however, we interpret it here as the transfer function (Neumann-to-Dirichlet map) of the block Stieltjes string terminated by a block Dirichlet condition. Replacing the termination condition 12 with a block Neumann condition,  $\mathcal{U}_{m+1} - \mathcal{U}_m = \mathbf{0}$ , introduces  $p$  eigenvalues at 0 and leads to a Gauß–Radau quadrature.

*Remark 1* [Interpretation of the the shift  $s$  as Laplace Variable  $s$  and  $\sqrt{s}$ ] The transition between diffusive and wave-type problems is handled through a reinterpretation of the shifted system with shift  $s$  as Laplace variable. In the diffusion case, we consider operators of the form  $(-\Delta + sI)$ , where  $s$  is the transform of the time derivative  $\partial_t$ . For the wave equation,  $(-\Delta + \hat{s}^2 I)$ , we define  $\hat{s} = \sqrt{s}$  to map the second-order temporal derivative  $\partial_{tt}$  into the same algebraic framework. This substitution allows us to interpret the same Stieltjes string representation from both perspectives, provided the spectral domain of interest is appropriately mapped.

### 3 Block Krein–Nudelman extension

Extending this analogy to problems arising from differential equations on a semi-infinite interval  $x \in [0, \infty)$ , Krein and Nudelman truncated the Stieltjes string using a finite-difference variant of the Sommerfeld radiation condition [19]. We write such a condition for  $p \geq 1$  in the form

$$(\sqrt{s}\phi)\mathcal{U}_{m+1} = -\frac{1}{\gamma_m}(\mathcal{U}_{m+1} - \mathcal{U}_m), \quad (15)$$

replacing the equation (12) in the block Stieltjes string. Here  $\phi \in \mathbb{R}^{p \times p}$  is some s.p.d. matrix parameter whose choice we discuss later.

Returning to the interpretation of [19] for scalar  $\phi$  and  $p = 1$ , we extend the problem from the finite interval  $[0, x_{m+1}]$  to the semi-infinite domain  $[0, \infty)$ . To do so, we first replace the mass distribution  $\mathbf{m}_m$  from equation (14) with

$$\hat{\mathbf{m}}_m = \mathbf{m}_m + \phi^2 \eta(x - x_{m+1}), \quad (16)$$

where  $\eta(\cdot)$  denotes the Heaviside step function. This leads to the governing ODE

$$-u_{xx} + s\hat{\mathbf{m}}_m u = 0, \quad (17)$$

subject to the boundary condition  $u_x(0) = -1$  and the condition at infinity  $u(\infty) = 0$  for  $s \in \mathbb{C} \setminus (-\infty, 0)$ .

On the tail interval  $[x_{m+1}, \infty)$ , this parametrization yields outgoing wave solutions of the form  $u(x) = \mathcal{U}_{m+1} e^{-\sqrt{s}\phi x}$ . Consequently, the condition

$$\phi\sqrt{s}u|_{x=x_{m+1}} = -u_x|_{x=x_{m+1}} \quad (18)$$

truncates the semi-infinite domain back to  $[0, x_{m+1}]$ . This expression is equivalent to the 1D Sommerfeld radiation condition, while the truncation in equation (15) serves as its finite-difference approximation using a one-sided derivative.

We denote the resulting leading block of a block Stieltjes corresponding to Equations (10,12,15)

$$\hat{\mathcal{F}}_m^\phi(s) = \mathcal{U}_1 = u(0)$$

and call  $\hat{\mathcal{F}}_m^\phi(s)$  the Krein–Nudelman quadrature.

*Remark 2* Condition (18) is a simplified variant of the two-term square-root terminator condition [11]. We chose (18) for simplicity of incorporating it in the first-order port-Hamiltonian framework used for adaptive choice of  $\phi$ , see Appendix D. However the two term square-root condition can be incorporated in the Krein–Nudelman framework via discrete external mass distribution  $\hat{\mathbf{m}}_m = \mathbf{m}_m + \phi^2 \sum_{i=0}^{\infty} h\delta(x_{m+1} + ih - x)$ , replacing (18) with  $\phi\sqrt{s + (0.5hs)^2}u|_{x=x_{m+1}} = -u_x|_{x=x_{m+1}}$ , according to formula (2). It can be viewed as a counterpart of (18) when the exterior domain with mass density  $\phi^2$  is discretized using equidistant finite-different grid with step  $h$  [28], and they coincide in the limiting case  $h \rightarrow 0$ . This two-term condition may yield a more accurate truncation with proper optimization of the two parameters — this may be a subject of future research.

### 3.1 Krein–Nudelman extension in terms of the tri-diagonal matrix and connection to Gauß–Radau quadratures

In the general case  $p \geq 1$  and using equation (15) we eliminate  $\mathcal{U}_{m+1}$  from the  $m$ -th equation of the block Stieltjes system (11) and obtain

$$\frac{1}{\gamma_{m-1}} (\mathcal{U}_m - \mathcal{U}_{m-1}) - \frac{1}{\gamma_m} \left( \left[ \frac{1}{\gamma_m} + \sqrt{s}\phi \right]^{-1} \frac{1}{\gamma_m} - I \right) \mathcal{U}_m + s\hat{\gamma}_m \mathcal{U}_m = 0.$$

Combining this with the remaining equations of the system (11) and symmetrizing the obtained matrix pencil, we obtain an expression for  $\hat{\mathcal{F}}_m^\phi(s)$  in terms of a block tridiagonal system

$$\hat{\mathcal{F}}_m^\phi(s) = E_1^T (\hat{T}_m^\phi(s) + sI)^{-1} E_1. \quad (19)$$

Here  $\widehat{T}_m^\phi(s)$  coincides with  $T_m$  except for the last diagonal element

$$\widehat{\alpha}_m^\phi(s) = \alpha_m - (\widehat{\kappa}_m)^{-T} \gamma_m^{-1} (\gamma_m^{-1} + \sqrt{s}\phi)^{-1} \gamma_m^{-1} (\widehat{\kappa}_m)^{-1}. \quad (20)$$

By construction, this yields a symmetric  $\widehat{\alpha}_m$  and  $\lim_{\phi \rightarrow \infty} \widehat{\mathcal{F}}_m^\phi(s) = \mathcal{F}_m(s)$ . The other limiting corresponds to the Gauß–Radau quadrature  $\widetilde{\mathcal{F}}_m(s)$  given by  $\lim_{\phi \rightarrow 0} \widehat{\mathcal{F}}_m^\phi(s) = \widetilde{\mathcal{F}}_m(s)$  as defined in [5].

In the cited work it was shown that  $\forall s \in \mathbb{R}_+$

$$\dots < \mathcal{F}_{m-1}(s) < \mathcal{F}_m(s) \leq \mathcal{F}(s) \leq \widetilde{\mathcal{F}}_m(s) < \widetilde{\mathcal{F}}_{m-1} < \dots . \quad (21)$$

The following proposition extends this bound to the Krein–Nudelman quadrature and shows that similar to Gauß and Gauß–Radau quadrature, it is a Stieltjes function; however, unlike those, it is not meromorphic.

**Proposition 1** *For  $0 < \phi < \infty$*

1.  $\widehat{\mathcal{F}}_m^\phi(s)$  *is a Stieltjes function with the branch-cut on  $\mathbb{R}_-$ ;*
2.  $\forall s \in \mathbb{R}_+$  *we obtain the two sided bound*

$$\mathcal{F}_m(s) \leq \widehat{\mathcal{F}}_m^\phi(s) \leq \widetilde{\mathcal{F}}_m(s). \quad (22)$$

The proof is given in Appendix B.3. Proposition 1 states that the exact solution and the Krein–Nudelman approximation satisfies the same two-sided bounds.

Finally, in Appendix B we introduce the block Stieltjes continued-fraction representation (B16) of  $\widehat{\mathcal{F}}_m^\phi(s)$  which matches  $2m - 1$  Stieltjes moments of  $\mathcal{F}(s)$ . The classical Krein–Nudelman extension [19] matches  $2m$  moments [19] without additional cost. Our Krein–Nudelman approximation can be adapted accordingly. However, it leads to an additional free matrix valued parameter complicating optimization presented in Section 4. Its benefits in testing are insignificant, yet, for completeness, we give it in Appendix C.

## 4 Selection of $\phi$ via maximization of energy outflow

It remains to choose the non-negative matrix parameter  $\phi$  that minimizes the “reflection” induced by the truncation of the Lanczos recursion. The main idea is to interpret the system as a Stieltjes string that is truncated by a damper  $\phi$  and to maximize the ratio of dissipated energy to the total stored energy in the system. While this ratio vanishes for both Gauß and Gauß–Radau quadratures, an optimal choice of  $\phi$  should yield a non-trivial positive semi-definite value. In Appendix D we link the block-Stieltjes string to port-Hamiltonian systems and give a detailed derivation.

First, we use the 1D Krein–Nudelman representation and its energy considerations to guide us in the optimal choice of  $\phi$ . Multiplying ODE (17) by  $u(x)^*$  (Hermite

conjugate) and integrating by parts on the interval  $[0, x']$ ,  $x' > 0$  we obtain

$$\widehat{\mathcal{F}}_m^\phi(s) = -u(0)[u_x(0)]^* = \int_0^{x'} [u_x(u_x)^* + s\mathbf{m}uu^*]dx - (u_xu^*)|_{x=x'}. \quad (23)$$

For  $x' = \infty$  and  $s \in \mathbb{C} \setminus (-\infty, 0)$  the last term vanishes and we obtain

$$\widehat{\mathcal{F}}_m^\phi(s) = \int_0^{x'} |u_x|^2 + s\mathbf{m}(x)|u|^2 dx,$$

which for  $s \notin \mathbb{R}_-$  and  $p = 1$  becomes the energy of the system or a stationary functional. If  $x' = x_{m+1}$  with the help of the radiation condition (18) we obtain

$$\widehat{\mathcal{F}}_m^\phi(s) = \int_0^{x_{m+1}} |u_x|^2 + s\mathbf{m}(x)|u|^2 dx + (\sqrt{s}\phi)(uu^*)|_{x=x_{m+1}}. \quad (24)$$

The last term of the RHS is related to the energy outflow due to the boundary truncation at  $x_{m+1}$ . So its maximization relative to the stored energy will bring about maximal damping of the Krein–Nudelman term.

We note that the transfer functions of these second-order problems are related to their first-order counterparts by a factor of  $\sqrt{s}$  (See Remark 1). For the latter, the dissipated and stored energies correspond to the real and imaginary parts of the transfer function, respectively; a standard result in dynamical systems theory [29]. A detailed derivation of this relationship is provided in Appendix D.

We thus consider the following optimization problem, solved via the Nelder–Mead simplex method in our numerical experiments [30],

$$\operatorname{argmax}_{\phi > 0} = \oint_{\Gamma} \left\| \left[ \Re \widehat{\mathcal{F}}_m^\phi \right]^{-1/2} \Im \widehat{\mathcal{F}}_m^\phi \left[ \Re \widehat{\mathcal{F}}_m^\phi \right]^{-1/2} \right\| ds, \quad (25)$$

with  $\|\cdot\|$  a matrix norm and  $\Gamma$  is a contour, closely encircling the sub-interval  $[-d, 0]$  of  $-A$ 's spectrum at a distance comparable with the spectral gaps, to avoid numerical problems due to the singularities of  $\widehat{\mathcal{F}}_m^\phi$  at Ritz values. The lower boundary  $d$  is chosen so that the spectral measure of  $-A$  approximates its exact continuous counterpart sufficiently well on the sub-interval, and  $[-d, 0]$  contains a sufficient number ( $>> p^2$ ) of Ritz values to avoid overfitting.

The symmetrization in equation (25) is intended for the MIMO case, where  $\widehat{\mathcal{F}}_m^\phi$  is a matrix-valued function. Maximizing the relative energy dissipation while preserving the  $2m - 1$  Stieltjes moments matched by the block Lanczos method shifts the poles of  $\mathcal{F}_m$  (the negative eigenvalues of  $T_m$ ) to the ones of  $\widehat{\mathcal{F}}_m^\phi$  (negative Krein–Nudelman eigenvalues of  $\widehat{T}_m^\phi(s)$  or linear eigenvalue problem form (D31)) from the negative real axis onto the second Riemann sheet ( $\Re \sqrt{s} < 0$ ). This effectively increases the domain of analyticity for the approximation, as illustrated in Figure 1.

Assuming matrix  $A$  approximates an operator with a continuous spectrum,  $\widehat{\mathcal{F}}_m^\phi$  approximates a function characterized by scattering resonances (poles) on the second

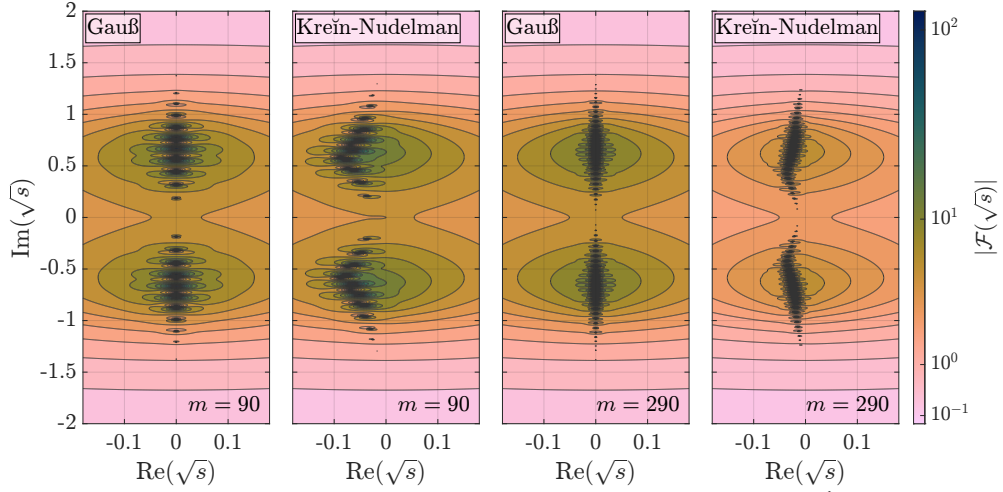


**Fig. 1:** This figure shows a contour plot of respectively  $\log |1 + \hat{\mathcal{F}}_m^\phi(s)|$  (Krein–Nudelman) and  $\log |1 + \mathcal{F}_m(s)|$  (Gauß) with  $p = 1$  (SISO) for  $m = 90$  (left) and  $m = 290$  (right) as a function of  $\sqrt{s}$  in the complex plane for the 3D Maxwell problem from subsection 5.2. To show both Riemann sheets in a single figure, the contours are shown as a function of the real and imaginary part of  $\sqrt{s}$ . The Gauß quadrature  $\mathcal{F}_m(s)$  is a single-valued function, thus it is even with respect to the imaginary axis, and as a function of  $\sqrt{s}$  has poles on the imaginary axis. Due to introduction of  $\sqrt{s}$  in the definition of the Krein–Nudelman quadrature  $\hat{\mathcal{F}}_m^\phi(s)$  it becomes a two-valued function (similar to the transfer function for the continuous problem), with the branch-cut at the imaginary axis and (scattering) poles at the second Riemann sheet  $\Re(\sqrt{s}) < 0$ . The dissipation optimization moves poles away from the branch cut adaptively; i.e. poorly converged Ritz values in the dense spectral area are moved further than converged well-separated Ritz values. This distance diminishes for the larger  $m$  together with the quadrature approximation error, thus the Krein–Nudelman poles approach the ones of the Gauß quadrature as  $m$  grows. The spectral measure at the branch cut is smooth in the area of poor convergence, collectively approximating the Stieltjes moments at dense intervals of  $A$ 's spectrum.

Riemann sheet [15]. The optimization improves the convergence until the approximation error becomes comparable to the error introduced by the discretization of the operator in  $A$ . This balance provides a reasonable stopping criterion. A similar approach proved successful in the optimization of perfectly matched layers [28]. While the reasoning presented here is intuitive, a rigorous mathematical justification is the subject of planned future work.

*Remark 3* During the optimization, we need to compute

$$Q^\phi(s) = (T_m + E_m \Delta \alpha_m^\phi E_m^T + sI)^{-1} E_1,$$

repeatedly for different  $\phi$ . Application of the Sherman–Morrison–Woodbury formula gives

$$Q^\phi(s) = (T_m + sI)^{-1} E_1$$

$$+ (T_m + sI)^{-1} E_m [((\Delta\alpha_m^\phi(s))^{-1} + E_m^T (T_m + sI)^{-1} E_m)^{-1} E_m^T (T_m + sI)^{-1} E_1$$

and thus we precompute

$$Q_m^m(s) = (T_m + sI)^{-1} E_m, \quad Q_m^1(s) = (T_m + sI)^{-1} E_1, \quad (26)$$

$$F_m^{m,m}(s) = E_m^T Q_m^m, \quad F_m^{1,m}(s) = E_m^T Q_m^1 \quad (27)$$

for all quadrature points used to discretize the integral in the optimization objective (25). Thus only  $p \times p$  systems have to be solved multiple times during optimization

$$Q^\phi(s) = Q_m^1(s) - Q_m^m(s)[(\Delta\alpha_m^\phi(s))^{-1} + F_m^{m,m}(s)]^{-1} F_m^{1,m}(s).$$

## 5 Numerical Examples

In this section, we apply our approach to three model problems in unbounded domains: 2D diffusion, the 3D quasistationary Maxwell's system, and the 2D wave equation.

A critical requirement for our method is that the matrix  $A$  is s.p.d. and accurately approximates the resolvent for  $s$  away from the negative real semi-axis. This allows us to use the block Lanczos algorithms without relying on absorbing boundary conditions or perfectly matched layers (PML), which would lead to non-Hermitian matrices.

Instead, we use the non-absorbing optimal grid with Dirichlet boundary conditions proposed in [31]. This grid follows a log-centered geometric progression with a progression factor of  $\exp(\pi/\sqrt{N_{\text{opt}}})$ , where  $N_{\text{opt}}$  denotes the number of grid points in the exterior domain.

Among all geometric progression grids, this choice yields the optimal convergence rate of  $\exp(-\pi\sqrt{N_{\text{opt}}})$  for the spectral measure over the optimization interval.<sup>1</sup>

The generic configuration combining a uniform interior grid with this optimal exterior grid is illustrated in Figure 2. Note that the figure depicts only the first steps of the exponentially expanding exterior grid, as the step sizes grow rapidly thereafter.

### 5.1 SISO 2D Diffusion test case

We discretize the symmetrized elliptic operator

$$A \approx -\sigma(\mathbf{x})^{-\frac{1}{2}} \Delta \sigma(\mathbf{x})^{-\frac{1}{2}} \quad (28)$$

on an unbounded domain using second-order finite differences over a  $300 \times 300$  grid with  $h = 1$ . To approximate this, we consider a Dirichlet problem on a bounded domain with  $N_{\text{opt}} = 10$  geometrically increasing grid steps in the exterior and a uniform grid in the interior part. This formulation is relevant to both heat transfer and the scalar 2D diffusion of electromagnetic fields, as well as to the wave propagation problem described in subsection 5.3.

The function  $\sigma(\mathbf{x})$  is illustrated in Figure 2. Here,  $B$  is represented as a vector of discrete delta functions with nonzero entries at the grid nodes corresponding to the transducer locations, labeled as  $Trx$  in the figure. In the  $p = 1$  Single-Input-Single-Output (SISO) results presented here, we only consider the first transducer.

---

<sup>1</sup>Superior rates can be achieved via Zolotarev or Neumann approximations [31]. Additionally, approximations more closely linked to interior finite-difference discretizations are proposed in [28], where they are also applied to the discretization of PML.

Figure 3 presents the results for this model with a single vector  $B$ , ( $p = 1$ ). At the initial superlinear convergence stage, the error is defined by the approximation of the well separated part of spectrum and the conventional Gauß approach is superior. However, both, the Gauß–Radau (GR) and the Krein–Nudelman (KN) formulations become competitive for the linear interval of convergence, where the error is dominated by the approximation of the almost continuous spectrum of matrix  $A$ . The arithmetic average of the Gauß and Gauß–Radau quadrature (GR avg.) is the average of two S-fractions and has a similar convergence rate. Thanks to its adaptive properties, the Krein–Nudelman method (a single S-fractions) shows generally better convergence than the averaged Gauß and Gauß–Radau, however, the latter is much smoother. In the future we plan to make the optimization routine used to find  $\phi$  in the Krein–Nudelman approach more robust since the oscillations observed in the convergence curve originate from a lack of robustness of the current optimization framework. A possibility of such an improvement follows from Figure 3-a, where the optimal  $\phi$  found by true error minimization (which we call “cheating” because the true solution is required) compares with the one found in our energy optimization framework. Averaging the  $\phi$  obtained for several iterations will lead to a better-behaved convergence, and the averaged  $\phi$  is close to the “cheated” curve.

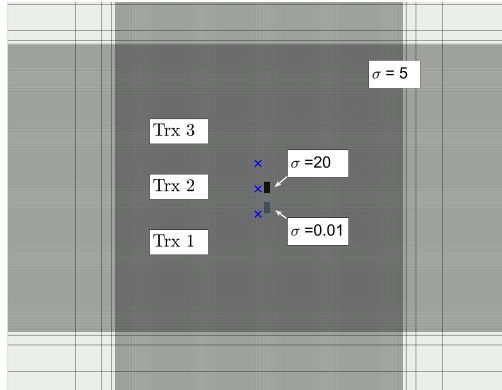
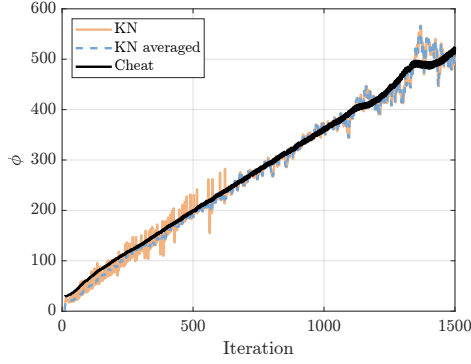


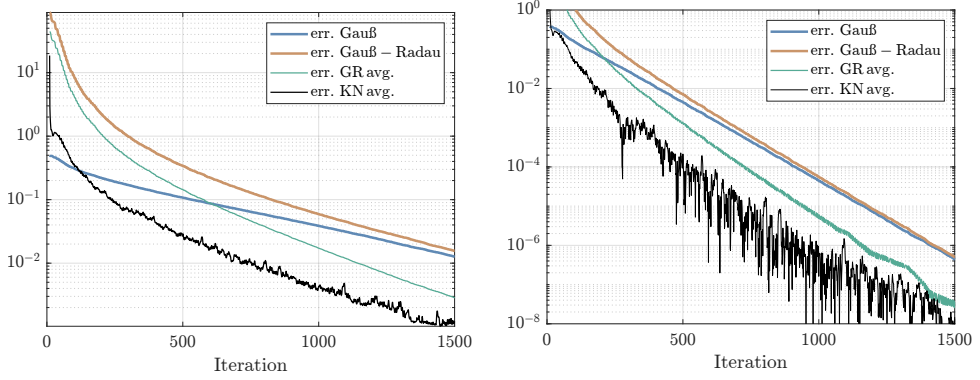
**Fig. 2:** Grid, heat conductivity  $\sigma(x)$  and transducer locations of the heat diffusion testcase. In the SISO results for  $p = 1$ , only transducer 1 is used. Only the first geometrically increasing grid steps are shown.

## 5.2 MIMO 3D Electromagnetic diffusion testcase

In this example, we consider the solution of the 3D Maxwell equations in the quasi-stationary (diffusive) approximation. Krylov subspace methods the computation of the action of matrix functions in this context were first introduced in [32] and remain a widely used approach in geophysical applications. The diffusive Maxwell equations



(a) Recovered values for  $\phi$  from dissipative energy maximization compared to the value of  $\phi$  that minimizes the distance to the true  $\mathcal{F}(s)$  for  $s \in [10^{-5} 10^0] \cup i[10^{-5} 10^0]$ . We call this the cheated  $\phi$



(b) Convergence for an imaginary  $s = 4 \cdot 10^{-5} i$ . (c) Convergence for a real  $s = 3 \cdot 10^{-4}$  value.

**Fig. 3:** Converge result for the 2D diffusion case in the SISO setting ( $p = 1$ ).

in  $\mathbb{R}^3$  can be rewritten as

$$(\nabla \times \nabla \times +\sigma(\mathbf{x})\mu_0 s)\mathcal{E}_{(r)}(\mathbf{x}, s) = -s\mathcal{J}_{(r)}^{\text{ext}}(\mathbf{x}, s), \quad \mathbf{x} \in \Omega, \quad (29)$$

where  $\sigma$  represents the electrical conductivity,  $\mu_0$  is the vacuum permeability, and  $\mathcal{J}_{(r)}^{\text{ext}}$  is the external current density associated with the transmitter index  $(r)$ , generating the electric field  $\mathcal{E}_{(r)}(\mathbf{x}, s)$ . For  $s \in \mathbb{C} \setminus (-\infty, 0)$ , the solution of (29) vanishes at infinity,

$$\lim_{\mathbf{x} \rightarrow \infty} \|\mathcal{E}(\mathbf{x})\| = 0. \quad (30)$$

To approximate the Maxwell equations (29)-(30), we employ the conservative Yee grid, following the methodology outlined in [32]. Similarly to the approach used for the

diffusion problem in  $\mathbb{R}^2$ , we truncate the computational domain by imposing Dirichlet boundary conditions on the tangential components of  $\mathcal{E}_{(r)}$  at the boundary. The grid is constructed with an optimally spaced geometric progression, ensuring spectral convergence of condition (30) at infinity. In our setup, we use  $N_{opt} = 6$  geometrically increasing grid steps with a scaling factor of  $\exp(\pi/\sqrt{6})$ , as proposed in [31]. The resulting grid consists of  $N_x = 80$ ,  $N_y = 100$ , and  $N_z = 120$  points, yielding a matrix  $A$  of size  $N = 2821\,100$ .

The conductivity  $\sigma$  is homogeneous and set to  $10^{-1}$  throughout the domain, except for two inclusions where  $\sigma = 10^{-3}$ , as shown in Figure 4. The excitation consists of six magnetic dipoles (approximated by electric loops): three positioned above the inclusions and three located at their center, as indicated by the arrows in Figure 4. This setup is analogous to the tri-axial borehole tools used in electromagnetic exploration geophysics [33, 34], leading to a matrix  $B$  with six columns.

Similarly to the results for the heat operator, the 3D results show an advantage of the Krein–Nudelman method and averaged Gauß and Gauß–Radau quadrature rules over stand-alone Gauß and Gauß–Radau on the linear interval of convergence. On this interval the error decays linearly due to the dense part of the spectral distribution. Overall, the Krein–Nudelman method shows best convergence, and due to the density of  $A$ ’s spectrum the convergence is much smoother.

In Figures 5a and 5b, the errors after  $m = 730$  block iterations are shown for a wide range of real and imaginary shifts, respectively. The Krein–Nudelman method performs best over the displayed frequency intervals. For a representative frequency in the middle of this interval, Figures 5c and 5d show the convergence behavior as the number of iterations increases.

The convergence behavior for the 3D case is more regular in our experience than in the 2D case, and  $\phi$  varies smoothly with the iterations, so averaging over iterations is not necessary. The discrete 3D operator has a denser spectral distribution, so the functional in the objective (25) is less affected by individual Ritz values which can be rather irregular due to instability of the simple block Lanczos algorithm in computer arithmetic. For simplicity, we optimized a scalar truncating factor  $\phi = \phi I_p$  for this MIMO case, as more complex parametrizations did not show immediate improvements.

### 5.3 Damped wave-propagation in unbounded domains via Krein–Nudelman extension

Square-root terminators were originally introduced in [35] to study the electronic band structure of materials, making many quantum-mechanical propagation problems computationally tractable in the 1970s. These early works relied on analytic atomic potential representations, where attaching a square-root terminator to the last computed fraction allowed the wave function to propagate “out” of the truncated area into an effective infinite medium, thereby preventing artificial reflections.

Let us consider the SISO variant of the 3D Maxwell’s problem from subsection 5.2 in the propagative (wave) regime. The solution for this case can be obtained with  $s = (\omega + \epsilon)^2$ ,  $\epsilon > 0$  when  $\omega > \epsilon$ , i.e., the propagative effects are dominant, and still  $\epsilon$  is large enough that the wave decays well in the exterior optimal grid (or for practical purposes the grid should be chosen large enough for the spurious reflections to

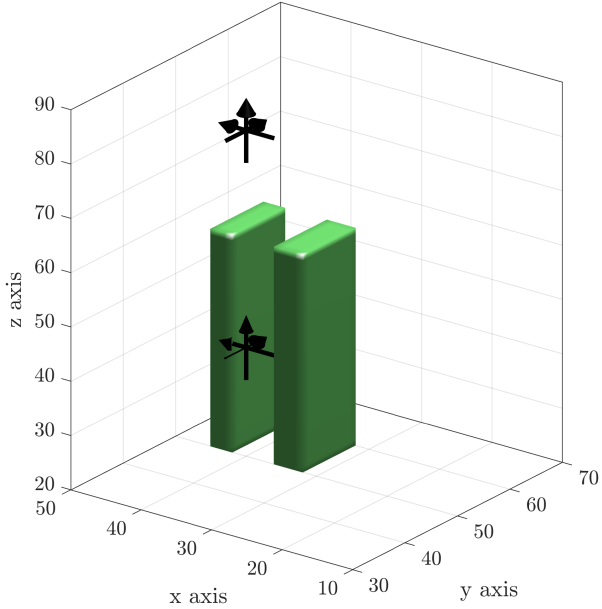


**Fig. 4:** 3D rendering of the simulated configuration with two inclusions for the tri-axial electromagnetic borehole tool,  $p=6$ .

be sufficiently small). This problem corresponds to electromagnetic propagation with harmonic frequency  $\omega$  in the lossy medium with dielectric permeability  $(1 - \frac{\epsilon^2}{\omega^2})\sigma$  and electrical conductivity  $2\epsilon\sigma$ . We present the convergence results of such a simulations in Figure 6. Compared to the cases presented in the previous subsection, the discreteness of the Lanczos spectral approximations has a stronger effect here and the Krein–Nudelman method significantly out-performs the discrete spectral approximations (Gauß, Gauß - Radau and their average) until the error reaches the level of the spurious reflected wave, which is of order  $10^{-2}$  relative to the exact solution. Then the discreteness of the Lanczos approximation and the exact spectral distribution become of the same level, and the averaged Krein–Nudelman method’s convergence slope becomes comparable to that of the other methods.

To illustrate the qualitative advantage of the Krein–Nudelman approximation, we consider experiments with the state solution  $(A + sI)^{-1}B$  for the 2D wave problem (not transfer functions as in the previous examples) using the same setup as in subsection 5.1, i.e., the same s.p.d. discretization  $A$  as in (28) and  $B$  in the SISO numerical example of subsection 5.1. We choose  $s \in \mathbb{C}$  close to the negative real semiaxis ( $\omega \gg \epsilon$ ) to show the effect of boundary reflections. We compute  $\Re Q_m(T_m + (\iota\omega + \epsilon)^2 I)^{-1}B \cdot \exp(\iota\omega t)$ ,  $\Re Q_m(\tilde{T}_m + (\iota\omega + \epsilon)^2 I)^{-1}B \cdot \exp(\iota\omega t)$ , and  $\Re Q_m(\tilde{T}_m^\phi(s) + (\iota\omega + \epsilon)^2 I)^{-1}B \cdot \exp(\iota\omega t)$  for respectively Gauß, Gauß–Radau and Krein–Nudelman quadratures, for  $m = 1000$  and  $m = 2000$  in, respectively, Figures 7 and 8. For or comparison we show the exact solution of the discretized problem

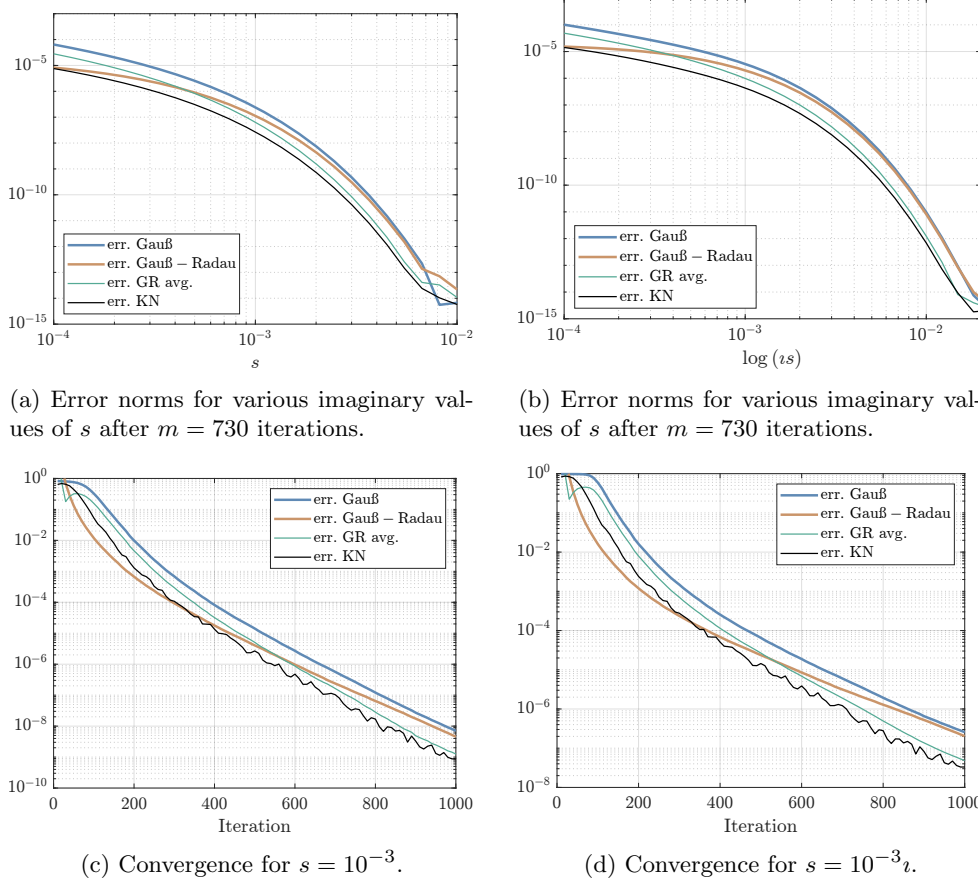


**Fig. 5:** Convergence results for the 3D EM case in the MIMO setting ( $p = 6$ ). As before “GR average” is arithmetic average of Gauß and Gauß–Radau quadratures.

$\Re(A + (\omega + \epsilon)^2 I)^{-1} B \cdot \exp(\omega t)$  in the rightmost column of both the figures. The top rows in these figures show 2D snapshots for a single  $t$ .

Let’s start with the case  $m = 1000$ . As shown in Figure 7, all three approximate solutions exhibit rather regular spherical wavefronts with noticeable scattering effects resulting from the inclusion. The exact solution, however, shows significant irregularity due to waves reflected from the Dirichlet boundary of the computational domain. On the lower row, the time evolution along the vertical cross-section indicated in the top row is shown. All solutions except the Krein–Nudelman solution exhibit standing-wave behavior, dominated by Ritz vectors or individual eigenmodes. This behavior is expected, since all three dynamics originate from discrete spectra with real eigenfunctions. In contrast, the Krein–Nudelman cross-section clearly captures an outgoing

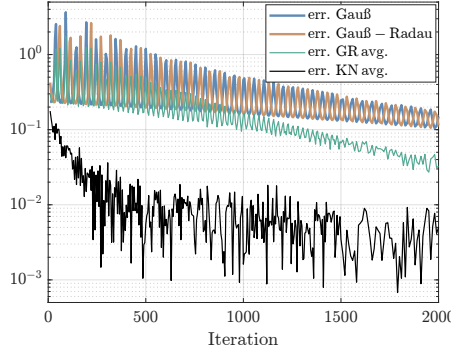


**Fig. 6:** Convergence in the wave propagation regime for the 3D electromagnetic problem (Subsection 5.2) with  $p = 1$ . The configuration uses only the central  $x$ -dipole from Figure 4, with  $s = -0.1 + 0.001i$  ( $\omega \approx 200\epsilon$ ). The legend is the same as in Figure 5. The Krein–Nudelman extension shows superior convergence before stagnating (in fact approaching the convergence speed of the other quadratures) at the level of spurious reflections.

wave propagating along the d'Alembert characteristics of the exact wave equation

$$-\sigma(\mathbf{x})^{-\frac{1}{2}} \Delta \sigma(\mathbf{x})^{-\frac{1}{2}} u + u_{tt} = 0,$$

thereby providing at least a qualitatively accurate approximation of the solution in an open domain, which is not possible with non-absorbing approximations.

Since the Stieltjes String for Gauß has a Dirichlet termination, the wave in the top panel of 7-A is terminated at a node. Conversely, the Gauß–Radau approximation leads to a termination at an antinode, a Neumann condition.

For the case  $m = 2000$  presented in Figure 8, snapshots of all three approximate solutions show increased irregularity. This arises because the discrete spectra have begun to converge to the exact operator's spectrum; consequently, the approximations move closer to the exact solution and further from the desired open-domain behavior.

Due to the convergent part of the discrete spectra, they are closer to the exact solution in the rightmost column and further from the desired outgoing wave behavior. The cross-section results in the bottom row for the Gauß and Gauß–Radau again show standing waves similar to the case with  $m = 1000$  (the exact solution is the same for both figures). The Krein–Nudelman waves for  $m = 2000$  are still dominantly outgoing — however, they have more irregularities due to convergent parts of the spectrum, contaminating the solution with standing waves. Eventually, as  $m \rightarrow \infty$  the Krein–Nudelman (as well as the other two approximate solutions) would converge to the exact solution, so it will again be just a superposition of standing waves. This change is consistent with the dependence of the scattering poles on  $m$  shown in Figure 1.

This situation is reminiscent of solving ill-posed linear systems by Krylov subspace iterations: while the fully converged solution can be highly sensitive to data errors, intermediate iterates often provide effective regularized approximations (see, e.g., [36]). We therefore can potentially adopt a similar strategy here, treating the

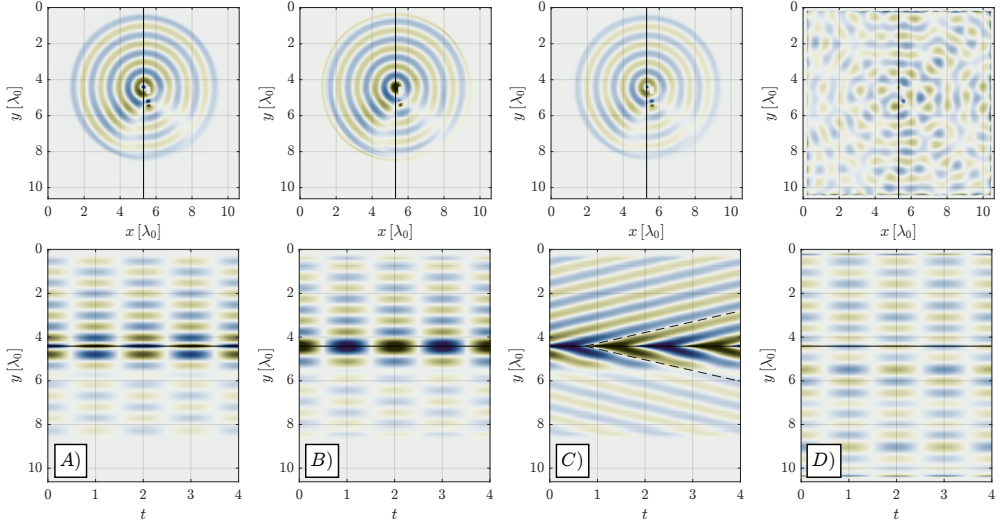


**Fig. 7:** Solution approximation of  $(A + (i\omega + \epsilon)^2 I)^{-1} B$  near the negative real semi-axis after  $m = 1000$  iterations. *Top Row:* Real part of the state solution for A) the Gauß, B) Gauß–Radau, C) Krein–Nudelman approximations, compared with D) the exact solution. *Bottom Row:* Time-domain evolution cross-sections sampled along the vertical black line. Only the Krein–Nudelman solution (C) exhibits propagating waves traveling along the d’Alembert characteristics (dashed lines). In contrast, the Gauß and Gauß–Radau approximations yield standing waves consistent with Dirichlet and Neumann boundary conditions, respectively — reflecting the specific truncation properties of the underlying Stieltjes string.

error of the discretization of the exterior domain as an error in the data. For robust wave-propagation computations using the Krein–Nudelman formulation, the number of iterations must be chosen carefully to avoid over-convergence. In particular, iterations should be terminated once the data misfit  $\|\hat{\mathcal{F}} - \mathcal{F}\|$  becomes comparable to the discretization error in the operator  $A$ . This requires reliable estimates of both error sources to define an appropriate stopping criterion.

## 6 Conclusions and Outlook

In this work, we have demonstrated that the approximation of matrix quadratic forms can be analyzed by rewriting the underlying Lanczos process as a matricial Stieltjes continued fraction. By interpreting this structure through the lens of block-Stieltjes strings, we establish a direct correspondence between the algebraic truncation of the Lanczos recursion and the physical behavior of a vibrating block-Stieltjes string. Specifically, we show that a block-Lanczos approximation at a finite iterate corresponds to a truncated string, which inherently introduces spurious reflections at the computational boundary.

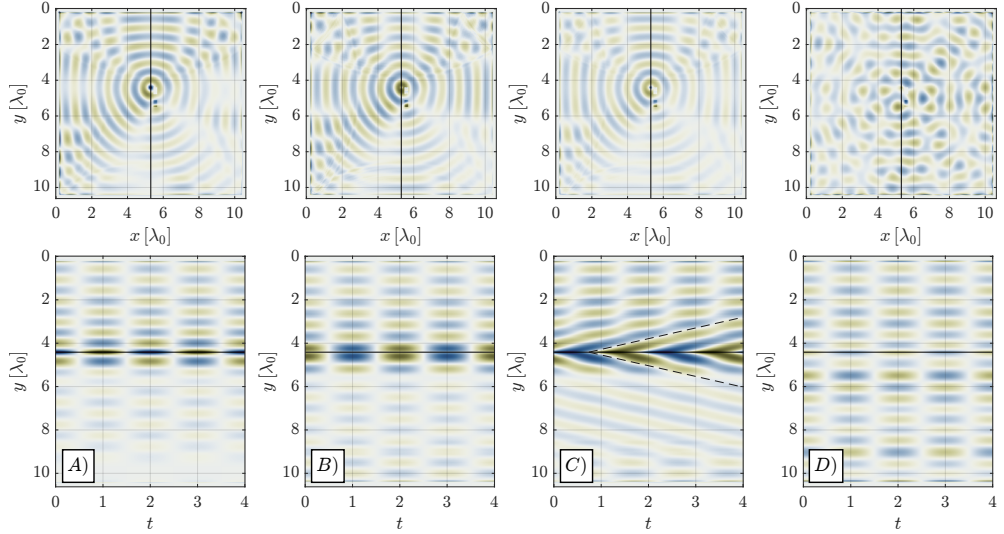


**Fig. 8:** Solution approximation for  $m = 2000$  iterations. Layout and parameters are identical to Figure 7. Note that all approximations now show boundary reflections due converging Ritz values and vectors.

We find that classical quadrature rules are characterized by specific boundary conditions: Gauß quadrature induces a Dirichlet-type reflection, whereas Gauß–Radau quadrature induces a Neumann-type reflection. Consequently, the averaging of these two rules as studied in [5] can be understood as an attempt to cancel these opposing non-absorbing boundary effects, i.e. they correspond to a superposition of a string with an even and odd extension.

To go beyond these classical limits, we proposed an absorbing boundary condition inspired by the Krein–Nudelman representation of rational Stieltjes functions. This boundary condition manifests as a term depending on the spectral parameter at the truncation point of the Stieltjes string, effectively introducing a branch cut in the resolvent. We term this method Krein–Nudelman method, which is a special case of the “square-root terminator” used in the quantum physics literature and effectively suppresses spurious reflections. This approach provides a superior framework for approximating matrices with almost continuous spectral distributions, particularly those arising from the discretization of PDE operators on unbounded domains, by allowing for spectral adaptation to scattering poles that remain inaccessible to the classical Lanczos method.

In the regime of linear convergence, both the Krein–Nudelman extension and the averaging of Gauß/Gauß–Radau quadrature rules yield significant error reductions when computing transfer functions for large-scale 2D diffusion and 3D quasi-stationary Maxwell systems. While the Krein–Nudelman approach consistently outperforms quadrature averaging in terms of absolute error, it exhibits a less regular convergence

profile. We hypothesize that this loss of monotonicity may be mitigated by refining the dissipation maximization procedure that we use to determine the optimal Krein–Nudelman damping parameter.

For wave propagation problems in unbounded domains, the Krein–Nudelman extension provides the strongest acceleration and also a qualitative correction to the solution by transforming nonphysical standing waves into the expected outgoing waves. However, this phenomenon can suffer from over-convergence as Ritz values converge, and finding an optimal stopping criterion consistent with the discretization error is required to make it robust.

Future research will focus on stabilizing the dissipation maximization procedure and extending the current scalar multiple of the identity matrix truncation  $\phi I_p$  to a matrix-valued parameter  $\phi$ . We intend to explore analytical methods for determining  $\phi$  alongside two-term square-root terminators to further accelerate convergence. Ultimately, a properly constructed terminator should allow the discrete operator spectrum to be effectively replaced by the scattering poles of its continuous counterpart, significantly improving convergence rates when these poles are well-separated from the branch cut.

Beyond optimizing the terminator itself, the proposed framework invites generalization to the approximation of matrix quadratic forms  $B^T f(A)B$  for a wider class of functions, such as the matrix exponential or Stieltjes functions. This could improve upon existing estimates based on Chebyshev series [37]. Moreover, as with the original square-root terminator [35], a natural application is the estimation of spectral densities for large matrices [38–40]. Here, the intrinsic continuous representation of spectral measures offers a distinct advantage over discrete approximations.

Another algorithmic avenue involves adopting the “stitching” method for preconditioning with the tail of a reference Lanczos recursion [14]. While this provides algebraic acceleration in quantum scattering, preliminary estimates for wave scattering with compactly supported perturbations suggest the potential for exponential or even superlinear convergence.

Finally, we anticipate that this approach extends to a broader class of problems exhibiting linear convergence, such as transfer function computations for large-scale graph-Laplacians [5]. Since randomized enrichment of the initial block is known to reduce block Lanczos iterations, we expect the Krein–Nudelman extension—with its superior spectral compression—to yield even stronger reductions. Consequently, combining this framework with randomized trace estimators [41, 42] represents another interesting direction for future work.

**Acknowledgements.** Vladimir Druskin was partially supported by AFOSR grants FA 9550-20-1-0079, FA9550-23-1-0220, NSF grant DMS-2110773 and Texas at Austin’s Deep Imaging Sub-Consortium (of the Research Consortium on Formation Evaluation), currently sponsored by AkerBP, Baker-Hughes, bp, ENI, Equinor ASA, Halliburton, and Petrobras. The computations were enabled by resources in project UPPMAX 2025/2-271 provided by Uppsala University at UPPMAX. Visualizations were created using scientific colormaps by Fabio Crameri [43].

## Ethics declarations

**Conflict of interest.** The authors declare that they have no conflict of interest, regarding the publication of this paper.

## Data Availability

Data sharing is not applicable to this article as no datasets were generated or analyzed during the current study.

## Appendix A Extraction of the Stieltjes parameters from the Lanczos block tridiagonal matrix

This appendix is included for completeness, for derivation, see [5, 25]. From the construction of  $\alpha_i$ 's and  $\beta_i > 0$  in Algorithm 1 we obtain that  $\hat{\kappa}_i, \gamma_i$  are full rank, as long as no deflation occurs in the block Lanczos recurrence, as  $\beta_i^T \beta_i > 0$  for  $i = 2, \dots, m$ , i.e. nonsingularity of all coefficients  $\alpha_i, \beta_i$  ensures that Algorithm 2 runs without breakdowns. For some scalings of problems, the extraction can be unstable if  $\hat{\gamma}_i$  or  $\gamma_i$  run off to zero and infinity, respectively, even though their product is stable. In such cases, it is possible to extract the parameters from  $\Delta\alpha_i$  and  $\beta_i$  by imposing that  $T_i - E_i \Delta\alpha_i E_i^T$  has a  $p$ -dimensional nullspace. From this condition,  $\Delta\alpha_i$  can be obtained using a  $(i-1) \times p$  dimensional block tridiagonal solve with  $p$  right-hand sides, by eliminating the last block row.

---

**Algorithm 2** Extraction algorithm  $\gamma/\hat{\kappa}$ :  
 (Block  $LDL^T$  Cholesky factorization of block tridiagonal  $T_m$ )

---

Given  $\alpha_i, \beta_i$  and  $\hat{\kappa}_1 = I_p$  (since  $\beta_1 = I_p$ )  
 $\gamma_1^{-1} = \hat{\kappa}_1^T \alpha_1 \hat{\kappa}_1$   
**for**  $i = 2, \dots, m$  **do**  
 $\hat{\kappa}_i^{-1} = -\gamma_{i-1} (\hat{\kappa}_{i-1})^T \beta_i^T$   $\triangleright (*)$   
 $\gamma_i^{-1} = (\hat{\kappa}_i)^T \alpha_i \hat{\kappa}_i - \gamma_{i-1}^{-1}$   $\triangleright (\dagger)$   
**end for**

---

Derivations of different variants of the Algorithm 2 are given in [5, 44]. We should point out that after  $m$  steps of the block Algorithm 1 one also can obtain  $\beta_{m+1}$  without additional multiplication by  $A$ , which allows us also to recover  $\hat{\kappa}_{m+1}$  and  $\hat{\gamma}_{m+1}$ .

## Appendix B Continued fraction interpretation

### B.1 Gauß ian quadrature

**Proposition 2** *The Gauß ian quadrature can be written as a truncated matricial Stieltjes continued fraction (S-fraction) :*

$$\mathcal{F}_m(s) = \cfrac{1}{s\hat{\gamma}_1 + \cfrac{1}{\gamma_1 + \cfrac{1}{s\hat{\gamma}_2 + \cfrac{1}{\ddots \cfrac{1}{s\hat{\gamma}_m + \cfrac{1}{\gamma_m}}}}}}, \quad (\text{B1})$$

where the basic building block of these S-fractions is given by the backward recursion

$$\mathcal{C}_i(s) = \cfrac{1}{s\hat{\gamma}_i + \cfrac{1}{\gamma_i + \mathcal{C}_{i+1}(s)}}, \quad \mathcal{C}_{m+1}(s) = 0, \quad (\text{B2})$$

with  $\mathcal{C}_i(s) \in \mathbb{C}^{p \times p}$ ,  $i = 1, \dots, m$  being s.p.d. for real positive  $s$ .

The proof for  $p = 1$  was known in Stieltjes work or even earlier, and its extension for  $p \geq 1$  is given in [5]. Here, for completeness, we present its simplified variant.

*Proof* To prove this statement we use induction. At every step of the induction, we increase the continued fraction and solve a block tridiagonal pencil problem that increases by one block each step and coincides with the full pencil  $(Z_m + s\hat{\Gamma}_m)$  at the last step. To facilitate this we define  $\mathcal{U}_i^j$  as a (triangular) family of  $p \times p$  real matrices

$$\{\mathcal{U}_i^j \in \mathbb{R}^{p \times p} | j = 1, \dots, m, i = j, \dots, m\},$$

where  $i$  corresponds to the blocks coupled through the three-term recurrence relation defined by the pencil  $(Z_m + s\hat{\Gamma}_m)$  and  $j$  corresponds to the steps of the induction where at the  $j$ -th step we enforce the (block Neumann) boundary condition

$$-\gamma_{j-1}^{-1}(\mathcal{U}_j^j - \mathcal{U}_{j-1}^j) = I_p. \quad (\text{B3})$$

This condition is enforced on the last  $m - j$  blocks of the three term recurrence relation defined by the  $m - j$  last block rows of  $(Z_m + s\hat{\Gamma}_m)$  which can be written out as

$$-\gamma_i^{-1}(\mathcal{U}_{i+1}^j - \mathcal{U}_i^j) + \gamma_{i-1}^{-1}(\mathcal{U}_i^j - \mathcal{U}_{i-1}^j) + s\hat{\gamma}_i \mathcal{U}_i^j = 0, \quad i = j, \dots, m, j = 1, \dots, m \quad (\text{B4})$$

$$\mathcal{U}_{m+1}^j = 0. \quad (\text{B5})$$

Note that for  $j = 1$  this corresponds together with (B3) to the full pencil problem  $(Z_m + s\hat{\Gamma}_m)[(\mathcal{U}_1^1)^T, \dots, (\mathcal{U}_m^1)^T]^T = E_1$ , which yields  $\mathcal{F}_m = \mathcal{U}_1^1$ .

Further, we introduce the notation

$$\mathcal{C}_j = \mathcal{U}_j^j \quad (\text{B6})$$

which due to condition (B3) provides the block-Neumann-to-Dirichlet map

$$\mathcal{C}_i[-\gamma_{i-1}^{-1}(\mathcal{U}_i^j - \mathcal{U}_{i-1}^j)] = \mathcal{U}_i^j \quad \forall i \geq j \quad (\text{B7})$$

since  $\mathcal{U}_{i \geq j}^j$  satisfies the same recursion  $\forall j$ . This holds because the sub-pencil for the tail  $i, \dots, m$  is invariant: the variables  $\mathcal{U}_i^j$  on this tail satisfy the same recurrence and boundary conditions as the intrinsic problem defining  $\mathcal{C}_i$ , regardless of the upstream driving index  $j$ .

As shown later during the induction, these maps are positive definite and thus invertible  $\forall s \in \mathbb{C} \setminus (-\infty, 0)$  and the inverse gives

$$-\gamma_{i-1}^{-1}(\mathcal{U}_i^j - \mathcal{U}_{i-1}^j) = \mathcal{C}_i^{-1}\mathcal{U}_i^j \quad \forall i \geq j \quad (\text{B8})$$

$$\leftrightarrow \mathcal{U}_{i-1}^j = (\mathcal{C}_i + \gamma_{i-1})\mathcal{C}_i^{-1}\mathcal{U}_i^j \quad (\text{B9})$$

which for  $i = j$  and assuming  $\gamma_i > 0$  and invertibility of  $\mathcal{C}_i$  gives

$$\mathcal{C}_{j+1}^{-1}\mathcal{U}_{j+1}^j = (\mathcal{C}_{j+1} + \gamma_j)^{-1}\mathcal{U}_j^j = -\gamma_j^{-1}(\mathcal{U}_{j+1}^j - \mathcal{U}_j^j). \quad (\text{B10})$$

With this in place consider the recursion (B4) for  $i = j$ , substitute the condition (B3) and replace the term  $-\gamma_j^{-1}(\mathcal{U}_{j+1}^j - \mathcal{U}_j^j)$  with the expression derived in (B10) to relate  $\mathcal{C}_{j+1}$  to  $\mathcal{C}_j$  as

$$(\mathcal{C}_{j+1} + \gamma_j)^{-1}\mathcal{C}_j + s\hat{\gamma}_j s\mathcal{C}_j = I_p \quad (\text{B11})$$

which gives the basic building block of the material S-fraction as

$$\mathcal{C}_j(s) = \frac{1}{s\hat{\gamma}_j + \frac{1}{\gamma_j + \mathcal{C}_{j+1}(s)}}, \quad \text{Re}\{s\} > 0. \quad (\text{B12})$$

We are now ready to perform the induction, where we show that indeed  $\mathcal{C}$ 's are invertible and that the upper recursion gives the desired S-fraction for  $\mathcal{F}_m$

- *Base Case:* For the case  $j = m$  the condition  $\mathcal{U}_{m+1}^m = 0$  implies  $\mathcal{C}_{m+1} = 0$  in (B12). Alternatively Equation (B4) for  $i = j = m$  can be written as

$$\gamma_m^{-1}\mathcal{C}_m + s\hat{\gamma}_m s\mathcal{C}_m = I_p \quad (\text{B13})$$

which starts the S-fraction as

$$\mathcal{C}_m(s) = \frac{1}{s\hat{\gamma}_m + \frac{1}{\gamma_m}}, \quad \text{Re}\{s\} > 0. \quad (\text{B14})$$

which is positive definite and thus invertible.

- *Induction Step:* Next for  $m > j \geq 1$  we assume that  $\mathcal{C}_{j+1}$  is positive definite such that

$$\mathcal{C}_j(s) = \frac{1}{s\hat{\gamma}_j + \frac{1}{\gamma_j + \mathcal{C}_{j+1}(s)}}$$

extends the S-fraction and ensures that  $\mathcal{C}_j$  is positive definite and invertible. The recursion ends with  $j = 1$  at which point (B3) and (B4) coincide with the full pencil.

□

## B.2 Extension to Gauß–Radau and Kreĭn–Nudelman quadratures

To obtain the continuous fraction expression for  $\widehat{\mathcal{F}}_m^\phi(s)$ , we return to the Gauß quadrature. Comparing equations (10–12) with (B2) we obtained ((B7)), the expression

$$\mathcal{C}_i^{-1}\mathcal{U}_i := -\frac{1}{\gamma_{i-1}}(\mathcal{U}_i - \mathcal{U}_{i-1}).$$

In the finite-difference interpretation of the block-Stieltjes string  $\mathcal{C}_i$  connects the solution  $\mathcal{U}_i$  with its backward differences, i.e.,  $\mathcal{C}_i^{-1}$  can be interpreted as the block Dirichlet-to-Neumann operator.

Condition (12) yields the last condition of (B2). Following [19, 45], and extending the Dirichlet-to-Neumann interpretation, we replace it with the “impedance boundary condition”

$$\mathcal{C}_{m+1}^{-1} := (\phi\sqrt{s}) \quad (\text{B15})$$

thus we obtain

$$\widehat{\mathcal{F}}_m^\phi(s) = \cfrac{1}{s\widehat{\gamma}_1 + \cfrac{1}{\gamma_1 + \cfrac{1}{s\widehat{\gamma}_2 + \cfrac{1}{\ddots \cfrac{1}{s\widehat{\gamma}_m + \cfrac{1}{\gamma_m + \cfrac{1}{\phi\sqrt{s}}}}}}}}. \quad (\text{B16})$$

Similar to the limiting transitions written in terms of the  $\widehat{T}_m^\phi(s)$ , we can write in terms of the continued fraction

$$\lim_{\phi \rightarrow \infty} \widehat{\mathcal{F}}_m^\phi(s) = \mathcal{F}_m(s) \quad (\text{B17})$$

and

$$\lim_{\phi \rightarrow 0} \widehat{\mathcal{F}}_m^\phi(s) = \cfrac{1}{s\widehat{\gamma}_1 + \cfrac{1}{\gamma_1 + \cfrac{1}{s\widehat{\gamma}_2 + \cfrac{1}{\ddots \cfrac{1}{s\widehat{\gamma}_m}}}}} = \tilde{\mathcal{F}}_m(s), \quad (\text{B18})$$

where  $\tilde{\mathcal{F}}_m(s)$  is the block Gauß–Radau quadrature as defined in [5].

## B.3 Proof of Proposition 1

Using the equations introduced in this appendix, we can now proceed with the proof of Proposition 1.

*Proof* To prove the first statement, we first notice that  $\sqrt{s}$  is a two-valued Stieltjes function with the branch cut on  $\mathbb{R}_-$ . Then  $\mathcal{C}_i$  are Möbius transforms of  $\mathcal{C}_{i-1}$ , so they recursively map the complex plane to itself and a Stieltjes function to another Stieltjes function. Thus recursively, the branch cut of  $\sqrt{s}$  is mapping to the branch cut with the same location.

The second statement is proved similarly to equation (21) in [5]. We write the counterpart of the recursion (B2) for  $\widehat{\mathcal{F}}_m^\phi(s)$  as

$$\begin{aligned}\widehat{\mathcal{F}}_m^\phi(s) &= \mathcal{C}_1(s), \\ \mathcal{C}_i(s) &= \frac{1}{s\widehat{\gamma}_i + \frac{1}{\gamma_i + \mathcal{C}_{i+1}(s)}}, \quad i = m, m-1, \dots, 1, \\ \mathcal{C}_{m+1}(s) &= (\phi\sqrt{s})^{-1}.\end{aligned}$$

By construction  $\mathcal{C}_{m+1}$  is strictly monotonic with respect to s.p.d.  $\phi^{-1}$  for  $s \in \mathbb{R}^+$ , and then  $\mathcal{C}_i$ 's are strictly monotonic with respect to  $\mathcal{C}_{i+1}$  for  $i = m, m-1, \dots, 1$ , which gives strict monotonicity of  $\widehat{\mathcal{F}}_m^\phi(s)$  with respect to  $\phi^{-1}$ . The Gauß quadrature is obtained in (B17) as the limit for  $\phi^{-1} \rightarrow 0$  so it gives the lower bound, and (B18) as the limit for  $\phi^{-1} \rightarrow \infty$ , so we obtain the Gauß–Radau quadrature as the upper bound.  $\square$

*Remark 4* To extend the first statement of Proposition 1 to  $p > 1$  one needs to extend the Möbius transform to matricial Möbius transforms (a.k.a. Linear Fractional Transformations (LFTs)). Then one needs to work with matrix-complex planes, which leads to a similar reasoning; however we leave a complete proof for future work.

The extension of the second statement of Proposition 1 to  $p > 1$  can be obtained by applying the monotonicity reasoning to the matrix-valued argument. Let  $\mathcal{F}_m(s, \mathcal{C}_{m+1}) = \mathcal{C}_1(s)$  be the lower recursion truncated by  $\mathcal{C}_{m+1}$

$$\mathcal{C}_i(s) = \frac{1}{s\widehat{\gamma}_i + \frac{1}{\gamma_i + \mathcal{C}_{i+1}(s)}}, \quad i = m, m-1, \dots, 1,$$

We consider three truncating values

$$\mathcal{C}_{m+1}^{\text{Gauß}}(s) = 0 < \mathcal{C}_{m+1}^{\text{Nudelman}}(s) = (\phi\sqrt{s})^{-1} < \mathcal{C}_{m+1}^{\text{Gauß–Radau}}(s) = \infty. \quad (\text{B19})$$

From

$$\frac{1}{s\widehat{\gamma}_i + \frac{1}{\gamma_i + \mathcal{C}_{i+1}(s)}} < \frac{1}{s\widehat{\gamma}_i + \frac{1}{\gamma_i + \mathcal{C}_{i+1}(s) + \tau}}, \quad \text{for } \tau > 0 \quad (\text{B20})$$

it directly follows that

$$\begin{aligned}\mathcal{F}_m(s, \mathcal{C}_{m+1}^{\text{Gauß}}(s)) &< \mathcal{F}_{m+1}(s, \mathcal{C}_{m+2}^{\text{Gauß}}(s)) < \mathcal{F}_m(s, \mathcal{C}_{m+1}^{\text{Nudelman}}(s)) \\ &< \mathcal{F}_{m+1}(s, \mathcal{C}_{m+2}^{\text{Gauß–Radau}}(s)) < \mathcal{F}_m(s, \mathcal{C}_{m+1}^{\text{Gauß–Radau}}(s)).\end{aligned}$$

## Appendix C Extended Kreĭn–Nudelman String

As noted before, computation of  $\beta_{m+1}$  at the  $m$ -th step of the block Lanczos algorithm does not require an additional matrix multiplication, allowing us to compute  $\widehat{\gamma}_{m+1} =$

$\widehat{\kappa}_{m+1}^T \widehat{\kappa}_{m+1}$  according to Algorithm 2. For that, we extend equation (11) by appending and equation for  $i = m + 1$  as

$$\frac{1}{\gamma_m} (\mathcal{U}_{m+1} - \mathcal{U}_m) - \frac{1}{\xi} (\mathcal{U}_{m+2} - \mathcal{U}_{m+1}) + s \widehat{\gamma}_{m+1} \mathcal{U}_{m+1} = 0, \quad (\text{C21})$$

replacing (15) with

$$(\sqrt{s}\phi) \mathcal{U}_{m+2} = -\frac{1}{\xi} (\mathcal{U}_{m+2} - \mathcal{U}_{m+1}), \quad (\text{C22})$$

where  $\xi \in \mathbb{R}^{p \times p}$  is a s.p.d. matrix.

We call the system (10,11, C21,C22) the “Extended Krein–Nudelman string”. We will define the extended Krein–Nudelman quadrature as

$$\mathcal{F}_m^{\phi, \xi} = \mathcal{U}_1,$$

with  $\mathcal{U}$  satisfying (10,11, C21,C22). Combining and symmetrizing this matrix pencil, we obtain

$$\widehat{\mathcal{F}}_m^{\phi, \xi}(s) = E_1^T (\widehat{T}_m^{\phi, \xi}(s) + sI)^{-1} E_1, \quad (\text{C23})$$

where  $\widehat{T}_m^{\phi, \xi}(s) \in \mathbb{R}^{p(m+1) \times p(m+1)}$  can be represented as

$$\widehat{T}_m^{\phi, \xi} = \begin{pmatrix} T_m & \beta_{m+1}^T \\ \beta_{m+1} & \widehat{\alpha}_{m+1}^{\phi, \xi}(s) \end{pmatrix}, \quad (\text{C24})$$

with

$$\widehat{\alpha}_{m+1}^{\phi, \xi}(s) = (\widehat{\kappa}_{m+1})^{-T} [\gamma_m^{-1} + \xi^{-1} - \xi^{-1}(\xi^{-1} + \sqrt{s}\phi)^{-1} \xi^{-1}] (\widehat{\kappa}_{m+1})^{-1}. \quad (\text{C25})$$

Now, it is easy to see that we can obtain Gauß–Radau approximant  $\tilde{\mathcal{F}}_{m+1}(s) = \lim_{\xi \rightarrow \infty} \widehat{\mathcal{F}}_m^{\phi, \xi}(s)$ , thus  $\widehat{\alpha}_{m+1}^{\phi, \infty}(s) = (\widehat{\kappa}_{m+1})^{-T} \gamma_m^{-1} (\widehat{\kappa}_{m+1})^{-1}$  and

$$\Delta \alpha(s) = \widehat{\alpha}_{m+1}^{\phi, \xi}(s) - \widehat{\alpha}_{m+1}^{\phi, \infty}(s) = (\widehat{\kappa}_{m+1})^{-T} [\xi^{-1} - \xi^{-1}(\xi^{-1} + \sqrt{s}\phi)^{-1} \xi^{-1}] (\widehat{\kappa}_{m+1})^{-1} \quad (\text{C26})$$

is an s.p.d. matrix if  $\phi, \xi$  are s.p.d.

## Appendix D Port-Hamiltonian interpretation of spectral smoothing

In this appendix, we offer a derivation of the objective function (25) used to find  $\phi$  in the Krein–Nudelman representation, based on a port-Hamiltonian interpretation of the system. The  $LDL$  decomposition of the block tridiagonal matrix from equation (6)

$$T_m := (\widehat{\mathbf{K}}_m^{-1})^T J_m \mathbf{\Gamma}_m^{-1} J_m^T \widehat{\mathbf{K}}_m^{-1}$$

allows us to rewrite the block tridiagonal systems of equations

$$\left[ \widehat{\mathbf{K}}_m^{-T} J_m^T \widehat{\mathbf{\Gamma}}_m^{-1} J_m \widehat{\mathbf{K}}_m^{-1} + sI \right] Q = E_1 \quad (\text{D27})$$

into “first-order” hyperbolic form. Here we interpret  $\widehat{\mathbf{\Gamma}}_m^{-1} J_m$ , and  $-\mathbf{\Gamma}_m^{-1} J_m^T$  as finite difference approximates of the derivative and  $\sqrt{s}$  as temporal Laplace variable. Then, using the variables  $U = \widehat{\mathbf{K}}_m^{-1} Q$  and  $(\mathbf{\Gamma}_m)^{-1} J_m^T U = -\sqrt{s} \widehat{U}$  we obtain

$$\left[ \begin{pmatrix} 0 & J_m \\ -J_m^T & 0 \end{pmatrix} + \sqrt{s} \begin{pmatrix} \widehat{\mathbf{\Gamma}}_m & 0 \\ 0 & \mathbf{\Gamma}_m \end{pmatrix} \right] \begin{pmatrix} U(\sqrt{s}) \\ \widehat{U}(\sqrt{s}) \end{pmatrix} = \begin{pmatrix} \frac{E_1}{\sqrt{s}} \\ 0 \end{pmatrix} \quad (\text{D28})$$

where we have used the fact that  $\widehat{\mathbf{K}}_m^T E_1 = E_1$ . This is a port-Hamiltonian system with skew symmetric structure matrix. We obtain the energy inside the system in terms of solutions  $Q = (T_m + sI)^{-1} E_1$  as

$$E_{\text{tot}} = \left( \|U\|_{\widehat{\mathbf{\Gamma}}}^2 + \|(s)^{-\frac{1}{2}} J_m^T U\|_{\mathbf{\Gamma}^{-1}}^2 \right) = \left( \|Q\|_{\widehat{\mathbf{\Gamma}}}^2 + (|s|)^{-1} \|Q\|_{T_m}^2 \right). \quad (\text{D29})$$

With  $U = [\mathcal{U}_1; \dots; \mathcal{U}_m]$  and  $\widehat{U} = [\widehat{\mathcal{U}}_1; \dots; \widehat{\mathcal{U}}_m]$ , we consider a generalized outflow boundary condition  $f(s)$  in the Krein–Nudelman extension

$$f(s)\mathcal{U}_{m+1} = -\frac{1}{\gamma_m}(\mathcal{U}_{m+1} - \mathcal{U}_m) = \sqrt{s}\widehat{\mathcal{U}}_m. \quad (\text{D30})$$

In this manuscript, we mainly consider  $f(s) = \phi\sqrt{s}$ . This specific outflow condition can be incorporated into the port Hamiltonian system via the transition  $\gamma_m \mapsto \gamma_m + (\phi\sqrt{s})^{-1}$  leading to

$$\left[ \begin{pmatrix} 0 & J_m \\ -J_m^T & 0 \end{pmatrix} + \begin{pmatrix} 0 & 0 \\ 0 & E_m \phi^{-1} E_m^T \end{pmatrix} + \sqrt{s} \begin{pmatrix} \widehat{\mathbf{\Gamma}} & 0 \\ 0 & \mathbf{\Gamma} \end{pmatrix} \right] \begin{pmatrix} U(\sqrt{s}) \\ \widehat{U}(\sqrt{s}) \end{pmatrix} = \begin{pmatrix} \frac{E_1}{\sqrt{s}} \\ 0 \end{pmatrix}. \quad (\text{D31})$$

For  $s$  on the negative real semiaxis the dissipated and stored energy can be obtained as respectively imaginary and real part of the first- order transfer function  $\frac{1}{\sqrt{s}}[\mathcal{F}^\phi(s)]$ , since that will be the right hand side of (D31) after multiplying the equation by the complex conjugate of the state. This property is well known in physics, see, e.g., [29].

With Laplace frequency  $\sqrt{s}$ , this system can be interpreted as both the mass-string-damper string (as in Krein–Nudelman theory) or an LCR transmission line terminated by a single (damping) resistor. For illustration, we will use the latter, with  $\mathcal{U}_i$  being the voltages across capacitors with capacitance  $\widehat{\gamma}_i$  and  $\widehat{\mathcal{U}}_i$  being the currents through inductors with value  $\gamma_i$ . The circuit diagram of such a transmission line is shown in Figure (D1).

## References

[1] Golub, G.H., Meurant, G.: *Matrices, Moments and Quadrature with Applications*. Princeton University Press, Princeton, NJ (2010)

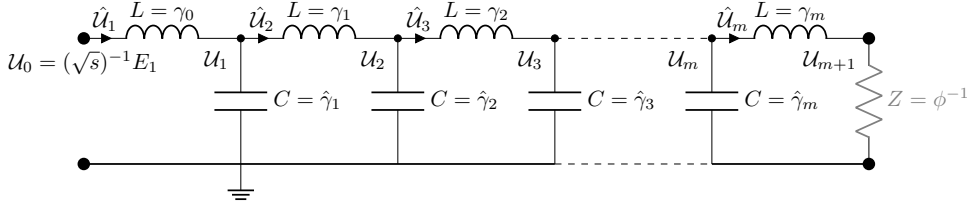


**Fig. D1:** Embedding of the block tridiagonal system (D31) as LC transmission line truncated with a single resistor. We give the values of the electrical impedance, equivalently, the transmission line can be built using inductors  $L_i = \gamma_i$ ,  $i = 0, \dots, m$ , capacitors  $C_i = \hat{\gamma}_i$ ,  $i = 1, \dots, m$ , and a single terminating resistor.

- [2] Reichel, L., Rodriguez, G., Tang, T.: New block quadrature rules for the approximation of matrix functions. *Linear Algebra and its Applications* **502**, 299–326 (2016)
- [3] Fenu, C., Martin, D., Reichel, L., Rodriguez, G.: Block Gauss and anti-Gauss quadrature with application to networks. *SIAM Journal on Matrix Analysis and Applications* **34**(4), 1655–1684 (2013)
- [4] Amsel, N., Chen, T., Greenbaum, A., Musco, C., Musco, C.: Near-optimal approximation of matrix functions by the Lanczos method. In: *Proceedings of the Thirty-Eighth Annual Conference on Neural Information Processing* (2024)
- [5] Zimmerling, J., Druskin, V., Simoncini, V.: Monotonicity, bounds and acceleration of block gauss and gauss–radau quadrature for computing  $b^t \phi(a)b$ . *Journal of Scientific Computing* **103**(1), 5 (2025)
- [6] López Lagomasino, G., Reichel, L., Wunderlich, L.: Matrices, moments, and rational quadrature. *Linear Algebra and its Applications* **429**(10), 2540–2554 (2008). Special Issue in honor of Richard S. Varga
- [7] Meurant, G., Tichý, P.: The behavior of the Gauss-Radau upper bound of the error norm in CG. *Numerical Algorithms* **94**(2), 847–876 (2023)
- [8] Lund, K.: A new block Krylov subspace framework with applications to functions of matrices acting on multiple vectors. Phd thesis, Department of Mathematics, Temple University and Fakultät Mathematik und Naturwissenschaften der Bergischen Universität Wuppertal, Philadelphia, Pennsylvania, USA (May 2018)
- [9] Haydock, R., Heine, V., Kelly, M.J.: Electronic structure based on the local atomic environment. *Journal of Physics C: Solid State Physics* **5**, 2845–2858 (1972)
- [10] Haydock, R.: The recursion method. *Solid State Physics* **35**, 215–294 (1980)
- [11] Beer, N., Pettifor, D.G.: Terminators for continued-fraction green’s functions in the recursion method. In: Phariseau, P., Temmerman, W.M. (eds.) *Electronic*

Structure of Complex Systems, pp. 769–777. Plenum Press, New York (1984)

[12] Beer, N., Pettifor, D.G.: The recursion method and the estimation of local densities of states. In: Phariseau, P., Temmerman, W.M. (eds.) The Electronic Structure of Complex Systems. NATO ASI Series, vol. 113, pp. 769–777. Springer, Boston, MA (1984). [https://doi.org/10.1007/978-1-4613-2405-8\\_14](https://doi.org/10.1007/978-1-4613-2405-8_14)

[13] Luchini, M.U., Nex, C.M.M.: A new procedure for appending terminators in the recursion method. *Journal of Physics C: Solid State Physics* **20**, 3125–3130 (1987)

[14] Pinna, G., Lunt, O., Keyserlingk, C.: Approximation theory for Green's functions via the Lanczos algorithm. arXiv (2025) <https://doi.org/10.48550/arXiv.2505.00089> [quant-ph]

[15] Dyatlov, S., Zworski, M.: Mathematical Theory of Scattering Resonances. Graduate Studies in Mathematics. American Mathematical Society, Providence, RI (2019)

[16] Krein, M.G.: The description of solutions of the truncated moment problem. *Matematicheskie Issledovaniya* **2**(2), 114–132 (1967)

[17] Krein, M.G.: On a generalization of stieltjes' investigations. *Doklady Akademii Nauk SSSR* **86**(6), 881–884 (1952)

[18] Krein, M.G.: The theory of extensions of semi-bounded hermitian operators and its applications. *Matematicheskii Sbornik* **20**, 431–495 (1947). Part I; Part II in vol. 21 (1947), pp. 365–404

[19] Krein, M.G., Nudelman, A.A.: Some spectral properties of a nonhomogeneous string with a dissipative boundary condition. *Journal of Operator Theory* **22**(2), 369–395 (1989)

[20] O'Leary, D.P.: The block conjugate gradient algorithm and related methods. *Linear Algebra and its Applications* **29**, 293–322 (1980). Special Volume Dedicated to Alson S. Householder

[21] Golub, G.H., Underwood, R.: The block Lanczos method for computing eigenvalues. In: Rice, J.R. (ed.) *Mathematical Software III*, pp. 361–377. Academic Press, New York (1977)

[22] Golub, G.H., Meuran, G.: *Matrices, Moments and Quadrature with Applications*. Princeton University Press, Princeton (2010)

[23] Knizhnerman, L.A.: The simple Lanczos procedure: estimates of the error of the Gauss quadrature formula and their applications. *Computational Mathematics and Mathematical Physics* **36**, 1481–1492 (1996)

[24] Greenbaum, A.: Behavior of slightly perturbed Lanczos and conjugate-gradient

recurrences. *Linear Algebra and its Applications* **113**, 7–63 (1989)

[25] Druskin, V., Mamonov, A.V., Zaslavsky, M.: Multiscale S-fraction reduced-order models for massive wavefield simulations. *Multiscale Modeling & Simulation* **15**(1), 445–475 (2017)

[26] Zimmerling, J., Druskin, V., Guddati, M., Cherkaev, E., Remis, R.: Solving inverse scattering problems via reduced-order model embedding procedures. *Inverse Problems* **40**(2), 025002 (2023)

[27] Meurant, G., Tichý, P.: Error Norm Estimation in the Conjugate Gradient Algorithm. Society for Industrial and Applied Mathematics, Philadelphia, PA (2024)

[28] Druskin, V., Güttel, S., Knizhnerman, L.: Near-optimal perfectly matched layers for indefinite Helmholtz problems. *SIAM Review* **58**(1), 90–116 (2016)

[29] Landau, L.D., Lifshitz, E.M., Pitaevskii, L.P.: Electrodynamics of Continuous Media, 2nd edn. Course of Theoretical Physics, Vol. 8. Pergamon Press / Butterworth-Heinemann, Oxford / New York (1984)

[30] Lagarias, J.C., Reeds, J.A., Wright, M.H., Wright, P.E.: Convergence properties of the nelder–mead simplex method in low dimensions. *SIAM Journal on Optimization* **9**(1), 112–147 (1998) <https://doi.org/10.1137/S1052623496303470>

[31] Ingerman, D., Druskin, V., Knizhnerman, L.: Optimal finite difference grids and rational approximations of the square root i. Elliptic problems. *Communications on Pure and Applied Mathematics* **53**(8), 1039–1066 (2000)

[32] Druskin, V., Knizhnerman, L.: A spectral semi-discrete method for numerical solution of 3D non-stationary problems in electrical prospecting. *Phys. Sol. Earth* **24**, 641–648 (1988)

[33] Saputra, W., Ambia, J., Torres-Verdín, C., Davydycheva, S., Druskin, V., Zimmerling, J.: Adaptive multidimensional inversion for borehole ultra-deep azimuthal resistivity. In: SPWLA Annual Logging Symposium, pp. 041–013005 (2024). SPWLA

[34] Zimmerling, J., Druskin, V., Davydycheva, S., Saputra, W., Torres-Verdín, C., Antonsen, F., Lotsberg, J.K., Rabinovich, M.: A targeted quadrature framework for simulating large-scale 3d anisotropic electromagnetic measurements. arXiv preprint arXiv:2511.17999 (2025)

[35] Pettifor, D.G., Weaire, D.L. (eds.): The Recursion Method and Its Applications. Springer Series in Solid-State Sciences, vol. 58. Springer, Berlin, Heidelberg, New York, Tokyo (1985)

- [36] Reichel, L., Sadok, H., Zhang, W.-H.: Simple stopping criteria for the lsqr method applied to discrete ill-posed problems. *Numerical Algorithms* **84**, 1381–1395 (2020)
- [37] Druskin, V.L., Knizhnerman, L.A.: Two polynomial methods of calculating functions of symmetric matrices. *USSR Computational Mathematics and Mathematical Physics* **29**(6), 112–121 (1989)
- [38] Ubaru, S., Chen, J., Saad, Y.: Fast estimation of  $\text{tr}(f(a))$  via stochastic lanczos quadrature. *SIAM Journal on Matrix Analysis and Applications* (2017) <https://doi.org/10.1137/16M1104974>
- [39] Colbrook, M.J., Horning, A., Townsend, A.: Computing spectral measures of self-adjoint operators. *SIAM Review* **63**(3), 489–524 (2021) <https://doi.org/10.1137/20M1333985>
- [40] Yi, J., Massatt, D., Horning, A., Luskin, M., Pixley, J.H., Kaye, J.: A high-order regularized delta-chebyshev method for computing spectral densities. *arXiv* (2025) <https://doi.org/10.48550/arXiv.2512.03149> arXiv:2512.03149 [math.NA]
- [41] Avron, H., Toledo, S.: Randomized algorithms for estimating the trace of an implicit symmetric positive semi-definite matrix. *Journal of the ACM* **58**(2) (2011) <https://doi.org/10.1145/1944345.1944349>
- [42] Persson, D., Chen, T., Musco, C.: Randomized block-krylov subspace methods for low-rank approximation of matrix functions. *arXiv preprint arXiv:2502.01888* (2025)
- [43] Crameri, F.: Scientific colour maps. *Zenodo* (2023). <https://doi.org/10.5281/zenodo.8409685> . <https://doi.org/10.5281/zenodo.8409685>
- [44] Druskin, V., Mamonov, A.V., Thaler, A.E., Zaslavsky, M.: Direct, nonlinear inversion algorithm for hyperbolic problems via projection-based model reduction. *SIAM Journal on Imaging Sciences* **9**(2), 684–747 (2016) <https://doi.org/10.1137/15M1039432>
- [45] Krein, M.G., Nudelman, A.A.: The Markov Moment Problem and Extremal Problems. Nauka, Moscow (1973). English translation: Translation of Mathematical Monographs, AMS, vol. 50, 1977